

IMPROVED CATALOGUE BUILD-UP AND MAINTENANCE THROUGH FILTERING AND SENSOR-BASED MANEUVER DETECTION AND ESTIMATION

Pietro Russo⁽¹⁾, Giorgio Isoletta⁽¹⁾, Roberto Opromolla⁽¹⁾, Giancarmine Fasano⁽¹⁾

⁽¹⁾ *Department of Industrial Engineering, University of Naples Federico II, 80125 Piazzale Tecchio 80, Napoli, Campania, Italy, Email: {pietro.russo2,giorgio.isoletta,roberto.opromolla,g.fasano}@unina.it*

ABSTRACT

Maneuver detection and estimation are crucial for preventing duplicate objects and understanding satellite behaviours, thus supporting the Resident Space Objects cataloguing activities. This paper presents a methodology integrating radar and optical sensor data with catalogue filtering to detect and estimate maneuvers in both LEO and GEO. In particular, it is conceived to handle multi-target scenarios and allows dealing with two scenarios: a Tracking Scenario, where measurement correlation with an object fails because of a maneuver, and a Surveillance Scenario, characterized by uncorrelated observations without any maneuvering candidate. It uses a filter based on orbital element differences in the first case, and a filter based on the Mahalanobis distance in the second case to include in the process all the possible maneuvering objects. Then, in both the scenarios, the maneuver is detected and estimated by leveraging track-to-orbit correlation and orbit-to-orbit correlation. Numerical tests carried out within a simulated operational environment demonstrate the method effectiveness in terms of accuracy and processing speed.

1 INTRODUCTION

The increasing number of Resident Space Objects (RSOs) in Near-Earth Orbital Environment poses several challenges in terms of space sustainability. According to the ESA Space Environment Report 2024 [1], the number of debris larger than 1 cm in size is more than 1 million, but only 35000 objects are being tracked (about 9100 active payloads and 26000 debris larger than 10 cm in size). Tracking and cataloguing RSOs are crucial for monitoring the space environment, understanding object behaviour, preventing collisions, predicting re-entries, and updating orbital states. These activities are further complicated by active satellites unknown maneuvers. When a new measurement track is obtained, a correlation with catalogue objects is performed to identify the

observed one and update its orbital state. However, this correlation can fail due to events such as fragmentations creating new unknown candidates, unknown maneuvers of catalogued objects, or the discovery of a new RSO. The detection and the estimation of maneuvers can cope with the second source of correlation errors, thus avoiding the duplication of objects and gaining a better understanding of their behaviour.

Different maneuver detection and estimation approaches have been proposed in the literature. The earliest research focuses on historical orbital data analysis, trying to detect anomalies in orbital elements variations through the examination of consecutive Two-Line Elements (TLEs) sets [2][3]. Another branch of research integrates maneuver detection into the orbit determination process, by developing maneuver detection filters based on the use of the Unscented Kalman Filter [4] and on Interactive Multiple Models (IMM) technique [5]. Other studies consider maneuver detection and estimation as an optimal control problem where the objective is to minimize the control effort required to reduce the observations discrepancies [6]. In this regard, an approach combining the optimal control theory and the concept of admissible region has also been proposed [7]. An alternative method adopts a heuristic and statistical approach consisting of analysing historical data about satellites maneuvers to solve the problem [8]. Recent works, instead, treat maneuver detection as part of the association problem between pre-maneuver orbit predictions and post-maneuver observations [9][10]. Most of these approaches to the problem of maneuver detection and estimation focus on a single object. Holzinger [6] and Serra [7] present methodologies for solving the multi-target association problem, by assuming that satellites usually perform optimal maneuvers.

The main contribution of this work consists in proposing an alternative technique to detect the maneuvering

objects and estimate their maneuvers in a multi-object scenario, where the source of the uncorrelated measurements tracks is unknown or uncertain, without any a-priori assumption on the maneuvering effort. By integrating sensors observation data (radar and optical) and correlation algorithms already presented in literature [9][10] with catalogue filtering techniques, the entire catalogue of RSOs is accounted for, but only the potential maneuvering objects are included in the process, thus increasing the accuracy of the method and speeding up the analysis at the same time. This method enables efficient handling of operational surveillance and tracking scenarios with multiple objects in both LEO and GEO orbital regimes.

The remainder of the paper is structured as follows. Section 2 presents the proposed maneuver detection and estimation architecture. Section 3 reports the results obtained in three simulated scenarios, two for LEO and one for GEO, and it discusses the achieved performance. Final remarks and indications about future work are reported in Section 4.

2 METHODOLOGY

This section presents the proposed methodology for RSOs maneuver estimation and detection. It integrates radar and optical observations with catalogue filtering techniques to detect maneuvering objects and estimate their maneuver entity. The entire pipeline is depicted in Figure 1.

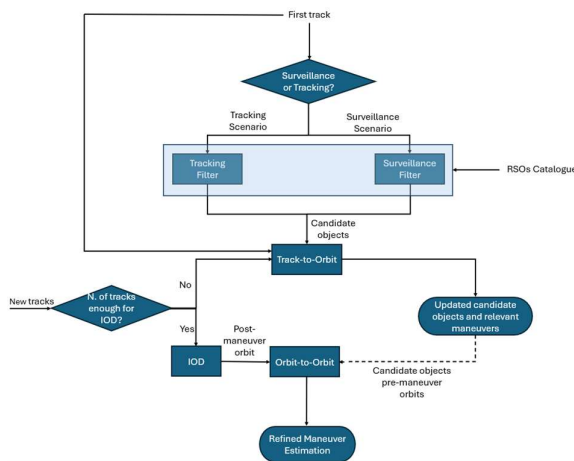


Figure 1. Maneuver detection and estimation methodology pipeline

A filter is applied to the catalogue to analyse only the

possible maneuvering objects according to the collected observations. Two cases are distinguished.

1) *Tracking Scenario*: observations correlation fails against the tracked object, which is then assumed to be the possible maneuvering object. In this case, a filter based on orbital elements differences with respect to the candidate maneuvering object is used.

2) *Surveillance Scenario*: one or more uncorrelated observations are found without any maneuvering candidate. A filter based on the Mahalanobis distance is applied.

The objects that pass the filters are processed as follows. A first guess of maneuvering object detection and maneuver estimate is obtained by associating the available uncorrelated tracks with each of the possible maneuvering RSOs orbits (track-to-orbit with maneuver hypothesis). Detection and estimation are refined as more tracks become available. If the estimated maneuvers of an object are above the maximum admissible maneuver magnitude, the object is removed from the process. Once the number of tracks is sufficient to initialize the post-maneuver orbit with reasonable accuracy, an orbit-to-orbit correlation is performed to further improve the accuracy of the results. In the following subsections each step of the process is described in detail.

2.1 Tracking Filter

In the *Tracking Scenario* an object is being tracked, but for some reason, it fails to correlate with an observation track that is expected to be generated by the object itself. If fragmentation events and the discovery of a new object are ruled out, the most likely explanation is an unknown maneuver. Although the tracked object is the primary candidate for maneuvering, a catalogue filter is developed to conservatively include in the process all the objects that are close to the tracked one at the observation epoch. This filter can be thought of as a six-dimensional box centred on the tracked object in the orbital parameters space. The size of the box is determined by the maximum allowable differences in orbital parameters (Table 1), selected according to a trade-off between the effects of the maneuvers analysed in this work (Table 3) and the orbital parameters of the majority of Resident Space Objects (RSOs).

Table 1. Maximum allowable differences in orbital parameters of tracking filter

Orbital Parameter	Δ
Semimajor axis, a	± 10 km
Eccentricity, e	10^{-3}
Inclination, i	$\pm 10^\circ$
Right Ascension of Ascending Node, Ω	$\pm 10^\circ$
Argument of Perigee, ω	$\pm 10^\circ$
True anomaly, ν	$\pm 10^\circ$

2.2 Surveillance Filter

The *Surveillance Scenario* is characterised by one or more uncorrelated tracks and no maneuvering candidates. In this case, there is no specific object which fails the correlation, but the track correlation fails against the entire catalogue. A direct approach to addressing the problem would be to apply the track-to-orbit function with maneuver hypothesis to all objects of the catalogue, by excluding unfeasible space objects and refining the solution as more tracks become available. To reduce the computational cost and speed up the process, a filter based on the Mahalanobis distance is used to keep only the possible maneuvering candidates in the process.

The Mahalanobis distance [11] is a metric used in multivariate statistics for correlation problems. Given two multivariate Gaussian independent variables, the real observation $\mathbf{X} \sim N(\mathbf{z}, \boldsymbol{\sigma}_m)$ and the predicted observation $\mathbf{Y} \sim N(\mathbf{h}, \boldsymbol{\sigma}_p)$, the Mahalanobis distance is a normalized distance defined as follows

$$Md = \sqrt{(\mathbf{z} - \mathbf{h})^T (\mathbf{C}_M + \mathbf{C}_p)^{-1} (\mathbf{z} - \mathbf{h})} \quad (1)$$

where \mathbf{z} is the vector of real observations; \mathbf{h} is the vector of predicted observations; \mathbf{C}_M is the measurement covariance matrix, containing the measurement variances; \mathbf{C}_p is the covariance matrix related to propagation uncertainty, which, for simplicity, is assumed to remain constant over time and equal to the latest known pre-maneuver orbital state uncertainty. Under these assumptions, the Mahalanobis distance follows a χ^2 distribution with k degrees of freedom, where k is the dimension of \mathbf{z} and \mathbf{h} (i.e., the number of different measurement types). This property allows the definition of a threshold Md_{th1} under which the two tracks are correlated with a given confidence level.

The working principle of the filter presented here is the

same, but it must take into account the possible maneuver the object has performed. Since there is no correlation between the measurement track and the catalogue objects if no maneuver is considered, a second threshold for Mahalanobis distance is statistically computed to detect the possible maneuvering object. In this way, if $Md < Md_{th1}$ there is correlation without maneuver; if $Md_{th1} < Md < Md_{th2}$ there is correlation with maneuver hypothesis; if $Md > Md_{th2}$ there is no correlation. In this work, we focus on finding Md_{th2} and the relevant confidence level. To compute Md_{th2} , a statistical analysis has been performed for both radar and optical measurements in LEO and only for optical observations in GEO. It consists in initializing 100 orbits with orbital parameters selected according to uniform random distribution in the ranges defined in Table 2, simulating a maneuver, and computing the Mahalanobis distance between the observations coming from the post-maneuver orbit and the ones deriving from the pre-maneuver orbit.

Table 2. Orbital parameters ranges

Orbital Parameter	LEO	GEO
Semimajor axis, a	[6878, 7770] km	[41378, 42684] km
Eccentricity, e	[0, 10^{-2}]	[0, 10^{-3}]
Inclination, i	[0, 180]°	[-10, 10]°
Right Ascension of Ascending Node, Ω	[0, 360]°	[0, 360]°
Argument of Perigee, ω	[0, 360]°	[0, 360]°
True anomaly, ν	[0, 360]°	[0, 360]°

For both LEO and GEO orbits, the ranges of orbital parameter values are chosen based on the majority of RSOs orbits in those regimes. Moreover, even though the values are randomly extracted for each orbit, in LEO semimajor axis and eccentricity are selected to ensure that the perigee altitude is above 200 km.

The maneuver is randomly selected among the ones in Table 3 and is performed in a given instant between the latest pre-maneuver orbital state epoch (UTC_{in}) and the initial epoch of measurement track (UTC_{meas_in}). These maneuvers are expressed in the RSW reference frame (radial component u_R , in-track component u_I , cross-track component u_C):

$$\hat{\mathbf{r}} = \frac{\mathbf{r}}{\|\mathbf{r}\|}, \hat{\mathbf{v}} = \frac{(\mathbf{r} \times \mathbf{v}) \times \mathbf{r}}{\|(\mathbf{r} \times \mathbf{v}) \times \mathbf{r}\|}, \mathbf{c} = \frac{(\mathbf{r} \times \mathbf{v})}{\|(\mathbf{r} \times \mathbf{v})\|} \quad (2)$$

where \mathbf{r} is the object position vector relative to the Earth and \mathbf{v} is the object velocity. For each component two representative maneuvers have been chosen, except for the in-track one, that is limited to the unitary magnitude, due to its larger effect on the time misalignment between the pre-maneuver and the post-maneuver orbital states.

Table 3. Maneuvers in RSW frame

Maneuver	u_R [m/s]	u_I [m/s]	u_C [m/s]
Radial	1	0	0
Radial	10	0	0
Cross-Track	0	0	1
Cross-Track	0	0	10
In-Track	0	1	0

For the analysis two different propagators have been used: a high-fidelity propagator, including all perturbations, to simulate the real orbit and the maneuver; a simpler propagator, including only drag and 4x4 gravity effects for LEO and third body and 4x4 gravity effects for GEO, for the reconstructed orbit and the predicted observations. The analysis has been repeated ten times in the three cases, obtaining the results in Figure 2 and Figure 3.

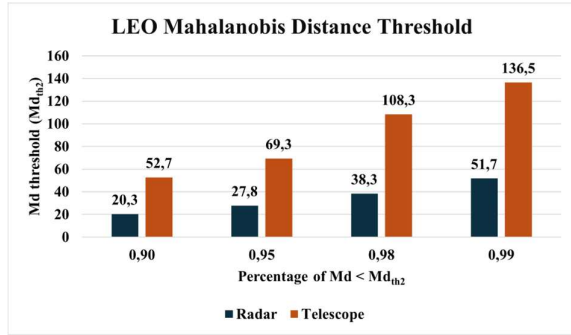


Figure 2. LEO Mahalanobis Distance threshold statistical analysis

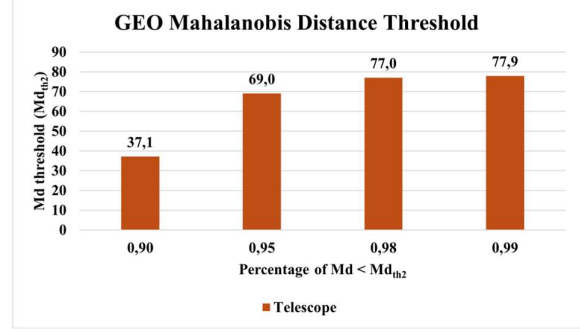


Figure 3. GEO Mahalanobis Distance threshold statistical analysis

As it is expected, due to the range-less nature and the more limited information content of optical observations, the quantiles of the telescope Mahalanobis distance distribution are larger than the radar Mahalanobis distance distribution quantiles. Depending on the orbital regime and type of observations, the corresponding quantile of order p , Md_p , can be used as a threshold for the surveillance filter. If $Md < Md_p$, the association with the maneuver hypothesis is accepted with a confidence level of p .

2.3 Track-to-orbit (T2O)

The maneuvering candidate objects (i.e., the objects passing the filter) are processed using the track-to-orbit (T2O) algorithm. This aims at providing a preliminary estimation of maneuver through a minimization of observation residuals $\boldsymbol{\rho} = \mathbf{z}(t) - \mathbf{h}(t, \mathbf{y}_B(t))$, which are the difference between the real measurements $\mathbf{z}(t)$ and the predicted measurements $\mathbf{h}(t, \mathbf{y}_B(t))$, derived from the reconstructed post-maneuver orbital state $\mathbf{y}_B(t) = [\mathbf{r}_B(t), \mathbf{v}_B(t)]^T$. The assumption is that an impulsive maneuver has been performed at a given instant $t_M \in T = [UTC_{in}, UTC_{meas, in}]$. Since the maneuvering time is unknown, the time interval T is discretized in a set of values t_M , and for each t_M the maneuver is estimated by minimizing the cost function

$$J = \frac{1}{N} \sum_{i=1}^N \boldsymbol{\rho}_i^T \mathbf{W} \boldsymbol{\rho}_i \quad (3)$$

where N is the number of measurements in a track and \mathbf{W} is the weighting matrix, i.e., the inverse of the expected variance of each measurement. The post-maneuver orbit \mathbf{y}_B is reconstructed by perturbing the pre-maneuver orbit \mathbf{y}_A with the maneuver \mathbf{u} through the Keplerian State Transition Matrix (STM) $\boldsymbol{\Phi}$ [12] (Eq. 4)

$$\mathbf{y}_B(t, t_M, \mathbf{u}) = \mathbf{y}_A(t) + \Phi(t, t_M)_v \mathbf{u} \quad (4)$$

By linearizing the problem around a reference maneuver \mathbf{u}^* , the maneuver $\mathbf{u} = \mathbf{u}^* + \Delta\mathbf{u}$ can be obtained by the iterative solution of the normal equation (Eq. 5)

$$(\mathbf{G}^T \mathbf{W} \mathbf{G}) \Delta\mathbf{u} = (\mathbf{G}^T \mathbf{W}) \Delta\mathbf{z} \quad (5)$$

$\Delta\mathbf{z}$ is the difference between the real measurements and the predicted measurements derived from the reference post-maneuver orbit $\mathbf{y}_B^*(t) = \mathbf{y}_b(t, \mathbf{u}^*)$; \mathbf{G} is the Jacobian matrix, containing the partial derivatives of measurements with respect to the estimated maneuver.

The output of track-to-orbit algorithm is a set of maneuvers for each object. A threshold value \mathbf{u}_{max} can be set to remove unfeasible maneuvers. If an object does not exhibit feasible maneuvers, it is removed from the process. The solution is refined as more tracks become available.

2.4 Orbit-to-orbit (O2O)

As the number of tracks is large enough to initialize with reasonable accuracy the post-maneuver orbit (it is proved that four is already a good number [13]), an orbit-to-orbit correlation is performed to improve the detection and estimate accuracy of the maneuvering object and the relevant maneuver. Given the pre-maneuver orbital state, $\mathbf{y}_A(t)$, and the post-maneuver orbital state, $\mathbf{y}_B(t)$, the Lambert's problem is solved for a set of $(t_{M1}, t_{M2}) \in T$ with $t_{M2} > t_{M1}$.

$$\begin{cases} \ddot{\mathbf{r}} + \frac{\mu}{r^3} \mathbf{r} = \mathbf{0} \\ \mathbf{r}_A(t_{M1}) = \mathbf{r}_1 \\ \mathbf{r}_B(t_{M2}) = \mathbf{r}_2 \end{cases} \quad \forall t_{M1}, t_{M2} \in T, t_{M1} < t_{M2} \quad (6)$$

The solution to Lambert's problem is the trajectory which connects the two orbits: $[\mathbf{r}_1, \mathbf{v}_1]$ and $[\mathbf{r}_2, \mathbf{v}_2]$. The output of the orbit-to-orbit algorithm is a set of two-impulses maneuver for each object $\Delta\mathbf{v}_1 = \mathbf{v}_1 - \mathbf{v}_A(t_{M1})$ and $\Delta\mathbf{v}_2 = \mathbf{v}_B(t_{M2}) - \mathbf{v}_2$. As for the T2O algorithm, a threshold value can be set to remove unfeasible maneuvers. In addition, even though the basic assumption of O2O is that a two-impulses maneuver has been performed, the propagation step can be reduced so that, among the O2O results, there will be maneuvers estimated for a very small Time of Flight (ToF) which can be assumed to be impulsive.

3 RESULTS

In this section the results are reported and discussed for two test cases:

- LEO satellite maneuver detection and estimation with both radar and optical observations in a surveillance scenario;
- GEO satellite maneuver detection and estimation with optical observations in a tracking scenario.

3.1 LEO test case

To reproduce a real surveillance scenario, the RSOs catalogue containing all the active LEO satellites is considered. The subject of this analysis is TIANQI-12 (NORAD ID: 48426), a small experimental LEO communication satellite from the Chinese Tianqi series. Real observations are simulated using a high-fidelity propagator, while predicted measurements are generated with a less accurate but faster propagator. The latest known pre-maneuver orbital state is assumed to be the one in Table 4; the first measurement track, lasting 10 minutes, is obtained 8 h later. Due to the uncertainties introduced using the Keplerian STM, at this stage of methodology development, the maneuver detection and estimation algorithm is applied only to objects whose latest known orbital state is within eight hours before the first track. Therefore, a pre-filtering step is performed to remove all the catalogue objects whose latest known orbital state falls outside this eight-hour window.

Table 4. TIANQI 12 latest pre-maneuver orbital state

Epoch	2024-12-11T02:00:29.191 UTC
ECI position, r	[-3874.14, 5751.18, 9.18] km
ECI velocity, v	[-5.14; -3.48; 4.37] km/s

A single impulse maneuver is performed by the satellite on $UTC_{man} = 2024 - 12 - 11T04:00:29.191$. The maneuvers considered for the test are the ones reported in Table 3. Three measurements tracks are considered for the analysis. The information about the tracks and the corresponding ground stations is reported in Table 5. It is important to note that the ground stations are simulated and do not correspond to real ones.

Table 5. LEO Scenario measurements tracks and ground stations

	Track 1	Track 2	Track 3
Length	10 min	8 min	6 min
Ground Station [lat, lon]	[15, 270] °	[-31, 116] °	[-7, 21] °
Epoch (UTC)	2024-12-11T10:00:00	2024-12-11T16:04:00	2024-12-12T00:14:00
Radar Noise	[0.005 km, 0.0005 km/s, 0.3°, 0.3°]		
Telescope Noise	[0.001°, 0.001°]		

3.1.1 Radar

Radar tracks consist of a set of four measurements (range, range rate, azimuth, elevation) taken every 5 seconds. When the first measurement track (Track 1) is received, following the missed correlation with all the objects of the catalogue (around 5000 objects), the surveillance filter is applied to the catalogue to detect the potential maneuvering objects. The results of the filter with $Md_{th2} = Md_{0.98}$ show that, regardless of the maneuver type and magnitude, the only object identified as a possible maneuvering object with a confidence level of $p = 0.98$ is TIANQI-12. These results are reported in Table 6.

Table 6. Surveillance filter results for radar observations at significance level $\alpha = 0.02$

Maneuver [RSW] m/s	Passed Objects [NORAD ID]	Md
[1, 0, 0]	48426	9.52
[10, 0, 0]	48426	16.78
[0, 0, 1]	48426	9.35
[0, 0, 10]	48426	0.97
[0, 1, 0]	48426	19.13

At this point, the potential maneuver object is analysed through the T2O algorithm, aiming to provide a preliminary estimate of the maneuver, which is refined as

more tracks become available. Figure 4 to Figure 6 show the results of the algorithm for the unitary cross-track maneuver with one, two, and three tracks, respectively. The vertical dashed line (blue) represents the real maneuver epoch, the horizontal one (black) is the real maneuver magnitude. Each red dot is a maneuver estimated at a given instant t of the time interval of analysis $T = [UTC_{in}, UTC_{meas_in}]$, where UTC_{in} is the epoch of the pre-maneuver orbital state of the object and UTC_{meas_in} corresponds to the time of the first track. As expected, the results exhibit a quasi-periodic behaviour and a higher number of tracks leads to a more accurate average estimation. Specifically, with only one track there are peaks which are one order of magnitude larger than the actual maneuver. Instead, with two or three tracks, the range of estimated maneuver magnitudes is closer to the true value. It is interesting to note that, regardless of the number of tracks, the maneuver magnitude at the true maneuver epoch is estimated with a relative error smaller than 15%. This point is used to compare the performance of the track-to-orbit algorithms for all the maneuvers considered in the test. The results reported in Table 7 refer to the maneuver estimation corresponding to the actual maneuver epoch. The maximum root mean square error of the estimated radial and cross-track maneuvers components, $RMSE = \sqrt{\frac{1}{3} \sum (v_{true,i} - v_{est,i})^2}$, is 0.3 m/s for the unitary maneuvers and 3 m/s for the maneuvers of magnitude 10. When a radial maneuver is performed, a non-negligible cross-track component is also estimated, but it decreases as more tracks are included in the loop. Furthermore, while estimation accuracy is generally expected to improve with additional tracks, this is not always the case due to the approximations and uncertainties introduced by the Keplerian STM. However, this trade-off between accuracy and computational speed is intentional, since the maneuver is estimated in less than one minute. The limitation of the track-to-orbit algorithm lies in the estimation of in-track maneuvers: due to the time-misalignment between the real observation tracks and the predicted ones caused by the maneuver, the algorithm compensates by overestimating the cross-track and the radial components.

Table 7. TIANQI-12 track-to-orbit algorithm results at maneuver epoch with radar tracks

Real Maneuver [m/s]	Est. Maneuver [m/s] – One track	Est. Maneuver [m/s] – Two Tracks	Est. Maneuver [m/s] – Three Tracks
[1; 0; 0]	[1.04; -0.002; 0.56]	[0.87; 0.002; -0.33]	[0.89; 0; 0.12]
[10; 0; 0]	[10.35; -0.01; -3.22]	[9.73; -0.001; -3.22]	[9.27; 0.004; 1.03]
[0; 0; 1]	[-0.005; 0; 1.009]	[0.007; 0; 1.13]	[-0.005; 0; 1.15]
[0; 0; 10]	[-0.013; 0.008; 10.40]	[0.07; 0.003; 11.44]	[-0.076; 0.006; 11.81]
[0; 1; 0]	[1.36; 0.97; 22.40]	[-3.23; 1.10; -16.70]	[-5.95; 1.08; 16.16]

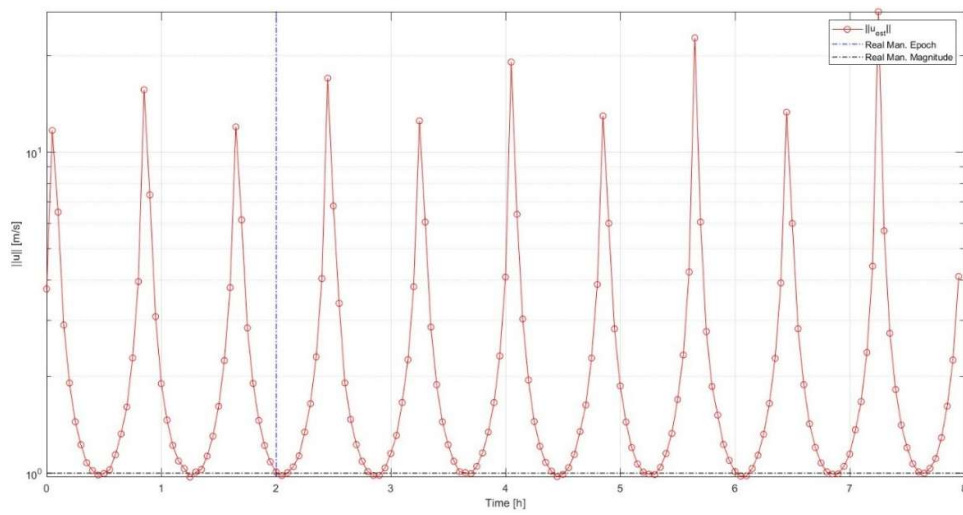


Figure 4. TIANQI-12 cross-track ([0 0 1] m/s) maneuver estimation with radar Track 1

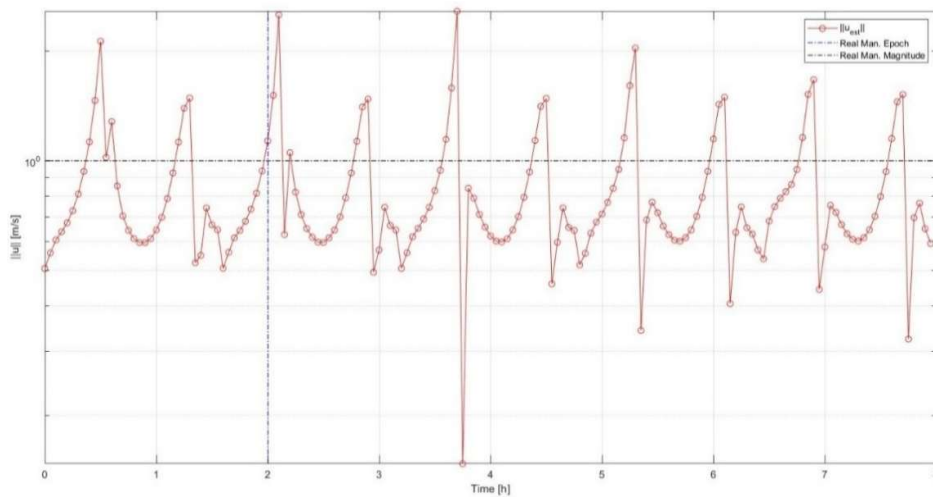


Figure 5. TIANQI-12 cross-track ([0 0 1] m/s) maneuver estimation with radar Track 1 and radar Track

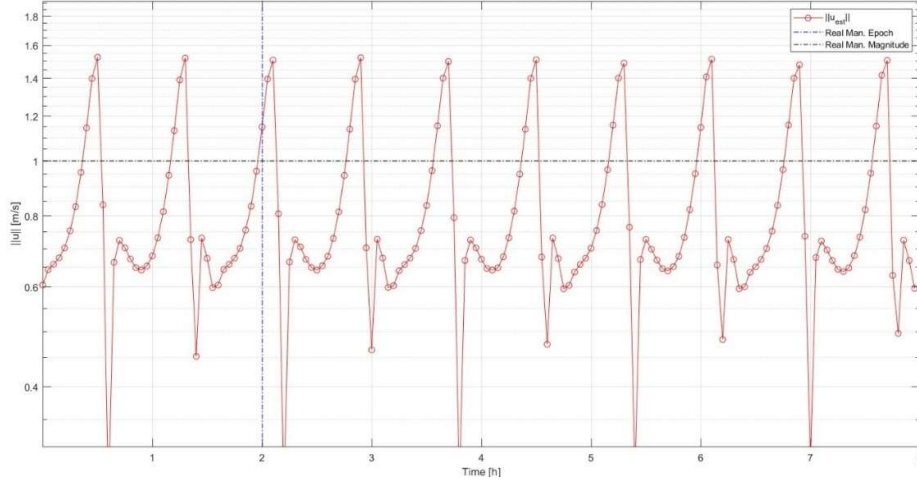


Figure 6. TIANQI-12 cross-track $[0\ 0\ 1]$ m/s) maneuver estimation with radar Track 1, radar Track 2 and radar Track

3

3.1.2 Telescope

Optical tracks consist of a set of two angular measurements (right ascension and declination) taken every 5 seconds. Unlike the radar scenario, the results of the filter with $Md_{th2} = Md_{0.98}$ show that there are different possible maneuvering objects with a confidence level of $p = 0.98$, due to the larger ambiguity of the optical observations with respect to the radar measurements. Table 8 summarizes these results.

Table 8. Surveillance filter results for optical observations at significance level $\alpha = 0.02$

Maneuver [RSW] m/s	Passed Objects	Md
	[NORAD ID]	
[1, 0, 0]	48426	2.06
	47967	32.6
[10, 0, 0]	48426	4.67
	47967	27.75
[0, 0, 1]	48426	2.71
	47967	34
[0, 0, 10]	55810	68.23
	48426	5.00
	47967	38.8
[0, 1, 0]	55810	64.12
	48426	17.57
	47967	10.88

Since more objects have passed the surveillance filter, the

track-to-orbit algorithm is used both as a filter and as a maneuver estimator. By selecting a threshold on the maximum admissible maneuver magnitude $u_{max} = 100$ m/s, it is possible to remove from the process all the objects without any estimated maneuver below this value. An example is presented in Figure 7 and Figure 8, corresponding to the unitary radial track maneuver. In this case, two satellites pass the surveillance filter: TIANQI-12 (NORAD ID: 48426) and M2-A Australian satellite (NORAD ID: 47967). Therefore, the track-to-orbit algorithm with Track 1 is applied to both satellites. Figure 7 shows the results for TIANQI-12, which are not so different from the ones obtained in the radar scenario (Figure 4). Figure 8, instead, depicts the results for M2-A. All the estimated maneuver magnitudes are well beyond the maximum admissible value and, so, the satellite is removed from the estimation process. As more tracks become available, the track-to-orbit algorithm is applied again to TIANQI-12 to improve the accuracy of maneuver estimation. Table 9 reports the maneuvers estimates at the actual maneuver epoch. The same considerations as the radar case can be made. However, despite the higher ambiguity of optical measurements, an accurate maneuver estimate is provided also in this case. The maximum RMSE of the estimated cross-track and radial maneuvers components is 0.1 m/s for the unitary maneuvers and 1 m/s for the maneuvers of magnitude 10.

Table 9. TIANQI-12 track-to-orbit algorithm results at maneuver epoch with optical tracks

Real Maneuver [m/s]	Est. Maneuver [m/s] – One track	Est. Maneuver [m/s] – Two Tracks	Est. Maneuver [m/s] – Three Tracks
[1; 0; 0]	[0.93; 0; -0.017]	[0.83; 0.003; 0.045]	[0.87; 0; 0.03]
[10; 0; 0]	[9.13; 0.01; 0.009]	[8.25; 0.04; 0.61]	[8.75; -0.001; 0.39]
[0; 0; 1]	[-0.01; 0; 0.97]	[-0.03; 0; 0.98]	[-0.02; 0; 1.004]
[0; 0; 10]	[-0.22; 0.01; 9.68]	[-0.38; 0.01; 9.98]	[-0.22; 0.009; 10.31]
[0; 1; 0]	[-3.93; 1.07; -0.84]	[-7.38; 1.18; 1.60]	[-8.50; 1.13; 0.53]

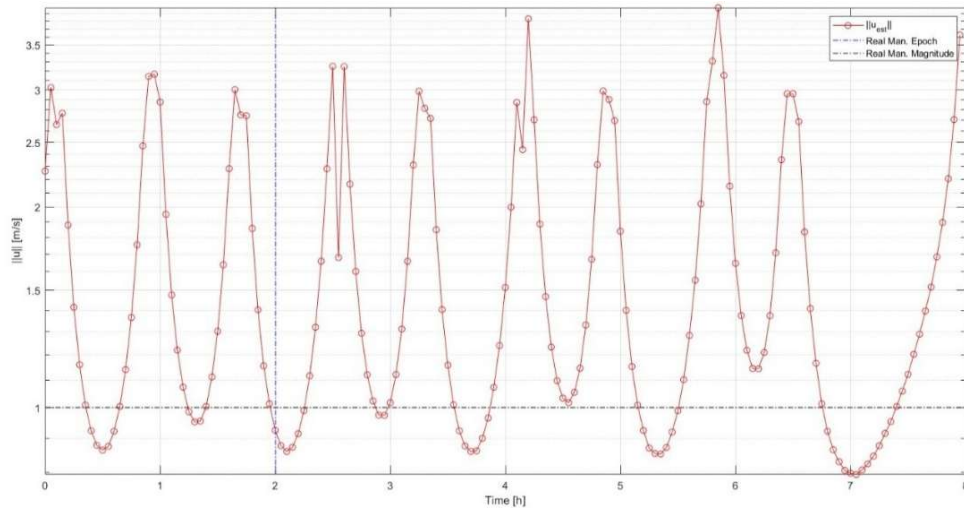


Figure 7. TIANQI-12 radial ($[1\ 0\ 0]$ m/s) maneuver estimation with optical Track 1

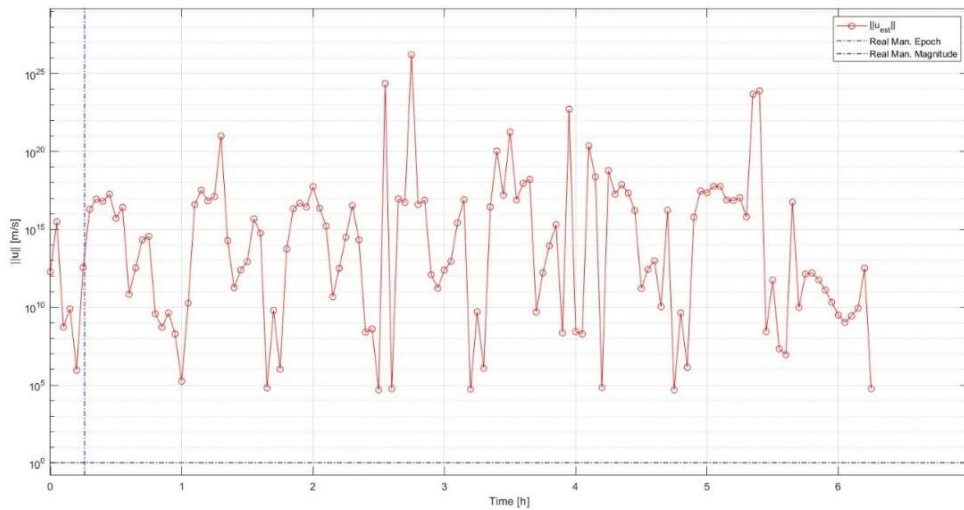


Figure 8. M2-A radial ($[1\ 0\ 0]$ m/s) maneuver estimation with optical Track 1

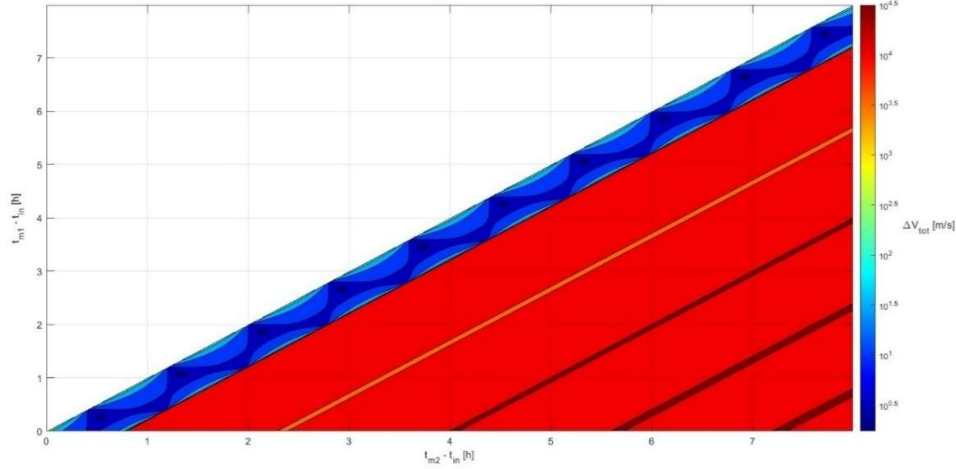


Figure 9. TIANQI-12 cross-track $([0\ 0\ 10]$ m/s) maneuver estimation with orbit-to-orbit algorithm

3.1.3 LEO Orbit-to-Orbit

As the number of tracks is large enough to initialize with good accuracy the post-maneuver orbit, an orbit-to-orbit correlation is performed to improve the accuracy of the maneuver estimation. The time interval T is discretized in a set of $(t_{M1}, t_{M2}), t_{M1} < t_{M2}$, where t_{M1} is the maneuvering time of the first impulse and t_{M2} is the maneuvering time of the second impulse. For each pair (t_{M1}, t_{M2}) the Lambert's problem is solved, and the maneuver is computed. Since the output is a two-impulse maneuver, the time step can be selected small enough to also estimate single-impulse maneuvers. Indeed, when two impulses are executed in consecutive time instants and are very close in time, they can be considered as a single impulse with good approximation. In LEO the time step is set to 30 s, because of a trade-off between accuracy and computational efficiency. Table 10 presents the results of the orbit-to-orbit algorithm at the actual maneuver epoch for TIANQI-12. As expected, the orbit-to-orbit algorithm enables more accurate maneuver estimation than the track-to-orbit algorithm. It also correctly estimates the in-track maneuver, overcoming the limitations of the track-to-orbit approach. However, small errors can still be found due to the Keplerian nature of the Lambert's problem, the selected time step and the orbit determination uncertainties. Figure 9 illustrates an example of maneuver estimation with the orbit-to-orbit algorithm. Each colour represents a specific order of magnitude for the estimated maneuver intensity, as

indicated by the colour bar on the right. To better interpret the results, the orbit correlation problem can be viewed as a targeting problem: starting from the pre-maneuver orbit, the interceptor must reach the post-maneuver orbit at a specific position at time t_{M2} . Diagonal bands of the same colour, tilted at a 45° angle, indicate that the order of magnitude of the estimated maneuvers is the same for a fixed ToF. However, the maneuver is identical only when the ToF and the relative geometry are the same. These maneuvers appear along the same diagonal band, separated in time by an interval equal to the *synodic period*: $\frac{2\pi}{\|n_{int} - n_{tgt}\|}$, where n_{int} is the mean angular motion of the pre-maneuver orbit and n_{tgt} is the mean angular motion of the post-maneuver orbit.

Table 10. TIANQI-12 maneuver estimation at the actual maneuver epoch with orbit-to-orbit algorithm

Real Maneuver [m/s]	Est. Maneuver [m/s]	RMSE [m/s]
[1; 0; 0]	[1.00; 0; -0.12]	0.071
[10; 0; 0]	[10.00; 0.009; -0.34]	0.194
[0; 0; 1]	[-0.004; 0.009; 0.66]	0.194
[0; 0; 10]	[-0.004; 0.012; 9.66]	0.194
[0; 1; 0]	[-0.004; 1.009; -0.34]	0.194

Table 11. INTELSAT-35E track-to-orbit algorithm results at maneuver epoch with optical tracks

Real Maneuver [m/s]	Est. Maneuver [m/s] – One track	Est. Maneuver [m/s] – Two Tracks	Est. Maneuver [m/s] – Three Tracks
[1; 0; 0]	[0.96; -0.099; 0.004]	[1.44; 0.007; -0.043]	[1.07; 0.079; 0.008]
[10; 0; 0]	[9.99; -0.017; 0.007]	[10.46; 0.023; -0.028]	[10.08; 0.096; 0.007]
[0; 0; 1]	[0.14; 0.43; 0.94]	[0.45; 0.006; 0.95]	[0.078; 0.079; 1.01]
[0; 0; 10]	[-0.011; -0.058; 10.00]	[0.45; 0.022; 9.96]	[0.078; 0.095; 10.00]
[0; 1; 0]	[0.049; 1.13; -0.031]	[0.45; 1.008; -0.038]	[0.002; 1.00; -0.007]

3.2 GEO test case

The subject of this analysis is INTELSAT-35E (NORAD ID: 42818), a geostationary satellite developed by Boeing Satellite Systems. As in the LEO scenario, real observations are simulated using a high-fidelity propagator, including all the perturbations, while predicted measurements are generated with a less accurate but faster propagator, including only the 4x4 gravity effects and third body perturbations. The latest known pre-maneuver orbital state is assumed to be the one in Table 12; the first measurement track, lasting 10 minutes, is obtained about 9 h later.

Table 12. INTELSAT-35E latest pre-maneuver orbital state

Epoch	2025-03-15T21:24:34.164 UTC
ECI position, r	[-6673.04; 41636.56; -12.27] km
ECI velocity, v	[-3.034; -0.49; 0.008] km/s

A single impulse maneuver is performed by the satellite on $UTC_{man} = 2025 - 03 - 15T03:24:34.164$. The maneuvers considered for the test are the ones in Table 3. Three measurements tracks are considered for the analysis. The information about the tracks and the corresponding ground stations is reported in Table 13. The selected ground stations are used by INTELSAT to monitor the satellite.

Table 13. GEO Scenario measurements tracks and ground stations

	Track 1	Track 2	Track 3
Length	10 min	10 min	10 min
Ground Station [lat, lon]	[40, 282] °	[50, 9] °	[43, 289] °
Epoch (UTC)	2025-03-15T07:00:00	2025-03-15T20:00:00	2025-03-16T07:00:00
Telescope Noise	[0.001°, 0.001°]		

3.2.1 Telescope

Optical tracks consist of a set of two angular measurements (right ascension and declination) taken every 5 seconds. Unlike the LEO analysis, a tracking scenario is simulated. Assuming the optical track fails the correlation with the tracked object (INTELSAT-35E), the tracking filter is applied to the catalogue containing all the GEO RSOs whose latest known orbital state is within twelve hours before the first track. As a result of the filter, the only object to be included in the process is INTELSAT-35E, which is the tracked object and, so, the primary candidate to have maneuvered. The potential maneuver object is analysed through the T2O algorithm, aiming to provide a preliminary estimate of the maneuver, which is then refined as more tracks become available. Figure 10 to Figure 12 show the results of the algorithm for the unitary in-track maneuver with one, two, and three tracks, respectively. Since the time interval

T of analysis is relatively small compared to the satellite orbital period, even the in-track maneuver is accurately estimated (the maximum RMSE is 0.26 m/s as for the radial and cross-track maneuvers). The periodic

behaviour does not emerge from these plots, because only a small portion of the orbit is analysed. For the same reason, the estimation accuracy is very high for all the tested maneuvers (Table 11).

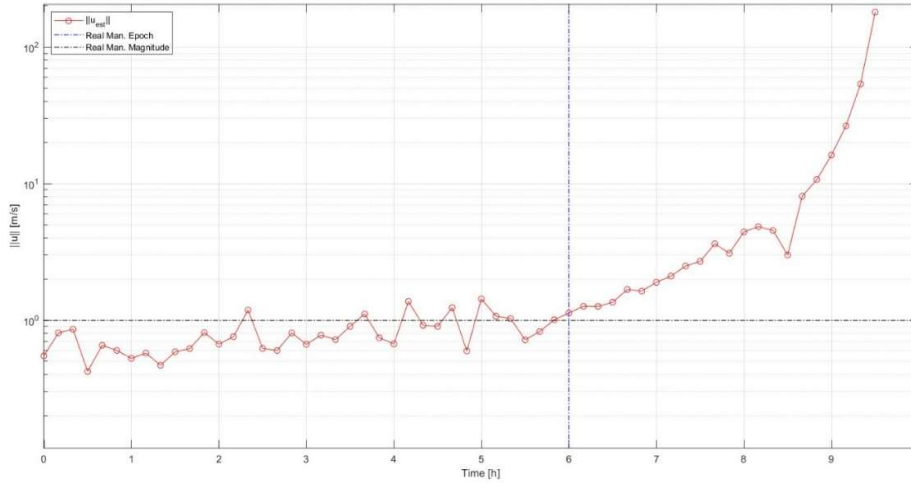


Figure 10. INTELSAT-35E in-track ($[0 \ 1 \ 0]$ m/s) maneuver estimation with optical Track 1

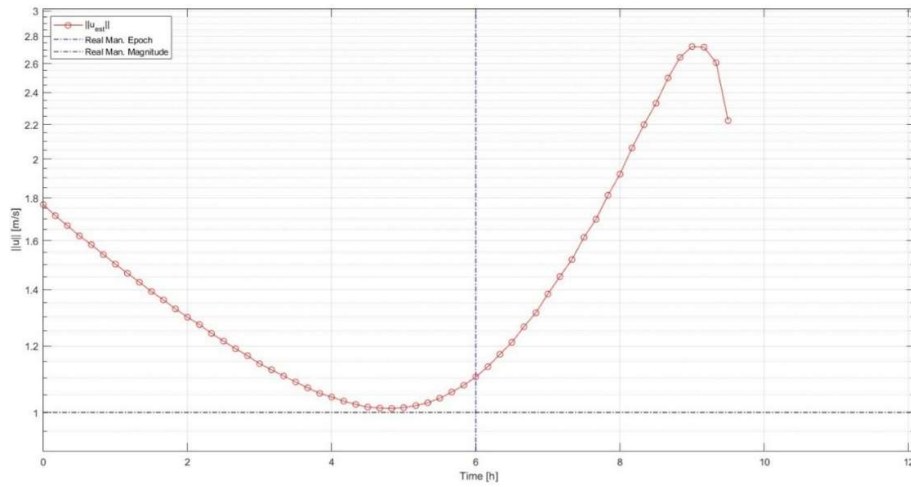


Figure 11. INTELSAT-35E in-track ($[0 \ 1 \ 0]$ m/s) maneuver estimation with optical Track 1 and optical Track 2

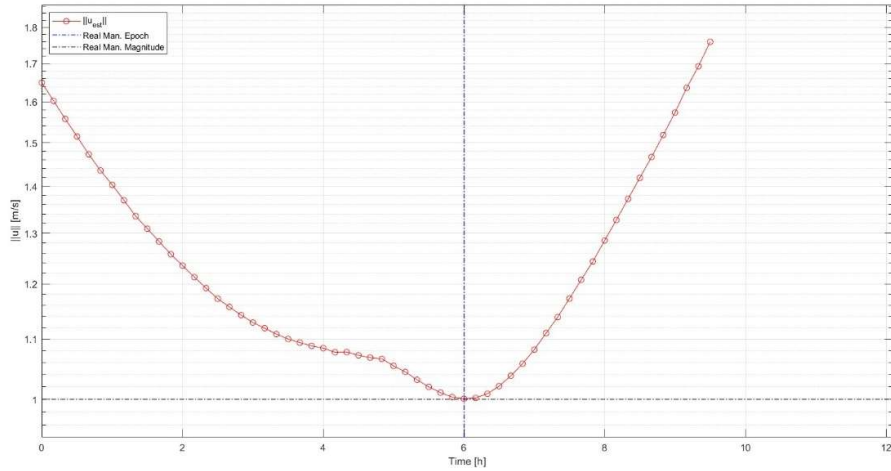


Figure 12. INTELSAT-35E in-track $[0 \ 1 \ 0]$ m/s) maneuver estimation with optical Track 1, optical Track 2 and optical Track 3

3.2.2 GEO Orbit-to-Orbit

Even in GEO, as the number of tracks is large enough to initialize with good accuracy the post-maneuver orbit, an orbit-to-orbit correlation is performed to improve the accuracy of the maneuver estimation. The higher orbital period of a GEO satellite allows to select a larger time step, by keeping the same level of approximation. In this analysis it is set equal to 60 s. The results reported in Table 14, corresponding to the maneuvers estimations at the actual maneuver epoch, exhibit a smaller RMSE than T2O estimations. Figure 13 presents an example of maneuver estimation in GEO with the orbit-to-orbit algorithm. The reason why the patterns characterizing the LEO orbit-to-orbit results are not so evident here is always related to the size of the time interval of analysis

with respect to the orbital period. To be clearer, this plot can be thought as a zoomed view of a plot regarding a much larger time interval T .

Table 14. INTELSAT-35E maneuver estimation with orbit-to-orbit algorithm

Real Maneuver [m/s]	Est. Maneuver [m/s]	RMSE [m/s]
[1; 0; 0]	[1.00; 0; 0]	0.0009
[10; 0; 0]	[10.00; 0; 0]	0.0012
[0; 0; 1]	[0.002; 0; 1.00]	0.0009
[0; 0; 10]	[0.002; 0.011; 10.00]	0.0067
[0; 1; 0]	[0.002; 1.00; 0]	0.0009

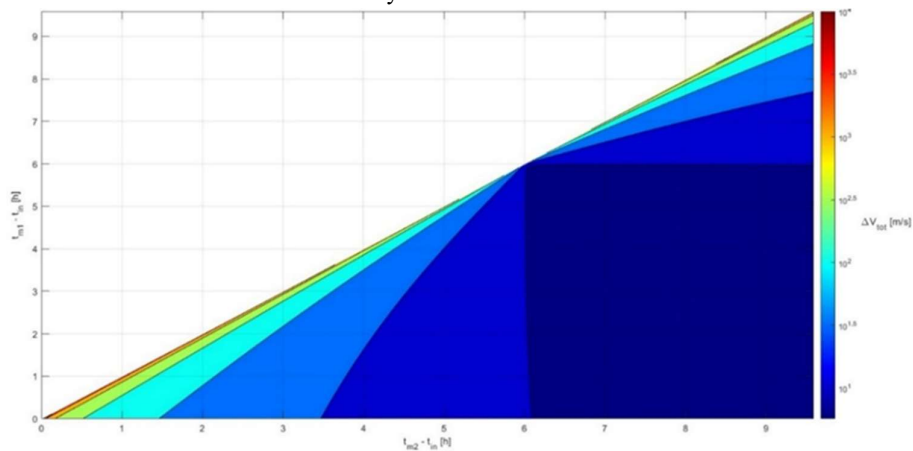


Figure 13. INTELSAT-35E radial $[10 \ 0 \ 0]$ m/s) maneuver estimation with orbit-to-orbit algorithm

4 CONCLUSIONS AND FUTURE WORK

This paper presented a methodology for real-time maneuver detection and estimation, integrating radar and optical observations with catalogue filters to handle multiple objects scenarios. It is designed for cases where a measurement track does not correlate with any catalogue object because of a potential maneuver. The proposed approach consists of three steps: catalogue filter, track-to-orbit algorithm, orbit-to-orbit algorithm. The first step aims to identify all the catalogue objects that may potentially have maneuvered. The track-to-orbit algorithm provides a preliminary maneuver estimation by correlating the real measurement tracks with the candidate maneuvering objects. A threshold on the maximum admissible maneuver magnitude can be set to filter out false positives. Finally, once enough uncorrelated tracks are available to initialize a post-maneuver orbit, the orbit-to-orbit algorithm refines the maneuver estimation through orbit correlation. Results demonstrate that this approach effectively detects maneuvering objects and estimates their maneuvers with good accuracy (small RMSE) in both LEO and GEO, while maintaining computational efficiency. The selected algorithm parameters ensure that each step executes in few minutes, making the methodology suitable for near real-time applications. Future work will focus on extending the methodology to larger time intervals of analysis and more complex maneuver scenarios, and on the combined use of optical and radar tracks for LEO satellites. Additionally, validation with real data will be conducted.

5 Acknowledgments

The research grant of Mr. Pietro Russo is funded by the Italian Space Agency (ASI) through “Attività tecnico-scientifiche di supporto a C-SSA/ISOC e simulazione di architetture di sensori per SST”.

6 References

1. European Space Agency (ESA). (2024). *ESA's Annual Space Environment Report*.
2. R.P. Patera. (2008). Space event detection method. In *Journal of Spacecraft and Rockets*, American Institute of Aeronautics and Astronautics Inc.
3. D. Hall, T. Kelecy, K. Hamada, & M.D. Stocker. (2007). *Satellite Maneuver Detection Using Two-line Elements Data Satellite Maneuver Detection Using Two-line Element (TLE) Data*.
4. J.M. Montilla, J.C. Sanchez, R. Vazquez, J. Galan-Vioque, J.R. Benayas, & J. Siminski. (2023). Manoeuvre detection in Low Earth Orbit with radar data. *Advances in Space Research* 72(7) 2689–2709.
5. G.M. Goff, J.T. Black, & J.A. Beck. (2015). Tracking maneuvering spacecraft with filter-through approaches using interacting multiple models. *Acta Astronautica* 114 152–163.
6. M.J. Holzinger, D.J. Scheeres, & K.T. Alfriend. (2012). Object correlation, maneuver detection, and characterization using control-distance metrics. In *Journal of Guidance, Control, and Dynamics*, American Institute of Aeronautics and Astronautics Inc.
7. R. Serra, C. Yanez, & C. Frueh. (2021). Tracklet-to-orbit association for maneuvering space objects using optimal control theory. *Acta Astronautica* 181 271–281.
8. G. Escribano, M. Sanjurjo-Rivo, J. Siminski, A. Pastor, & D. Escobar. *MANEUVER DETECTION VIA COMBINED HEURISTICAL AND STATISTICAL METHODOLOGIES*.
9. A. Pastor, G. Escribano, M. Sanjurjo-Rivo, & D. Escobar. (2022). Satellite maneuver detection and estimation with optical survey observations. *Journal of the Astronautical Sciences* 69(3) 879–917.
10. L. Porcelli, A. Pastor, A. Cano, G. Escribano, M. Sanjurjo-Rivo, D. Escobar, & P. Di Lizia. (2022). Satellite maneuver detection and estimation with radar survey observations. *Acta Astronautica* 201 274–287.
11. G.Y. McLachlan. (1999). Mahalanobis Distance. *Springer Resonance* 4 20–26.
12. O. Montenbruck, & E. Gill. (2000). *Satellite Orbits: Models, Methods and Applications*, Springer Berlin Heidelberg.
13. K. Hill, C. Sabol, & K.T. Alfriend. *Comparison of Covariance-Based Track Association Approaches Using Simulated Radar Data*.